BERGISCHE
UNIVERSITÄT
WUPPERTAL

Faculty of Mathematics
and Natural Sciences
Chair of Physics

Bachelor Thesis

Investigation of Afterpulse Phenomena in Photomultiplier Tubes for the Surface Scintillator Detectors at the Pierre Auger Observatory

submitted by

Patrik Rubelowski
Wuppertal, September 11, 2024

to obtain the degree
Bachelor of Science
in Physics

University of Wuppertal
Faculty of Mathematics and Natural Sciences
Summer Semester 2024

Advisor: Dr. Julian Rautenberg
First Examiner: Prof. Dr. Karl-Heinz Kampert
Second Examiner: Prof. Dr. Christian Zeitnitz

Contents

Abstract

This Bachelor Thesis investigates afterpulse phenomena in Photomultiplier Tubes used for the surface scintillator detectors at the Pierre Auger Observatory. Given the large amount of data, scripts were developed for analyzing and visualization of measurements, employing statistical methods to identify potential afterpulses. This research managed complications, notably distinguishing numerous irrelevant signals from those directly related to afterpulses. The results of these incidental findings were crucial to refine the data filtering process and finally examine the traces needed for afterpulse investigations.

Chapter 1

Introduction

The Pierre Auger Observatory is the largest observatory for the study of high-energy cosmic rays and has significantly advanced our understanding of Ultra-high Energy Cosmic Rays (UHECRs). Their definitive origin still remains unclear and the mechanisms of their creation remain a significant scientific challenge. Research lacks of identifiable sources of UHECRs and they outreach the possibilities of particle accelerators.

Over its 15 years of operation, covering an area of 3000 km^2, the Pierre Auger Observatory has achieved a significant exposure of approximately $60,000$ km^2 sr year. This substantial exposure has led to the collection of over $215,000$ events, creating an extensive dataset. This dataset has enabled high statistical precision in the measurement of UHECRs. [1] Since the Pierre Auger Prime upgrade, scintillator surface detectors (SSDs) equipped with photomultiplier tubes (PMTs) have been installed. Therefore, it is crucial to continue analyzing their performance and to maintain precision in their fine-tuning. The most critical aspect of analyzing afterpulses is to distinguish them from event-related actual pulses and to refine the measurements accordingly.

1.1 Motivation

This work focuses on the detection of afterpulses in PMTs. Since afterpulses can interfere with data by overlapping with genuine cosmic ray events, understanding this phenomenon is crucial for identifying inaccurate measurements. Consequently, this study contributes to ongoing research and aims to enhance data accuracy.

Chapter 2

Theory

2.1 Photomultiplier Tubes

PMTs are highly light-sensitive vacuum tubes. The primary function of PMTs is to detect photons, to convert them into electric signals and to amplify this signal. The PMTs achieve this through a photocathode that emits electrons upon photon impact, utilizing the photoelectric effect[2]. To accelerate these electrons towards the anode, a voltage is applied to create an electric field that attracts the electrons to the anode. The range of the applied voltage is specified by the manufacturer.

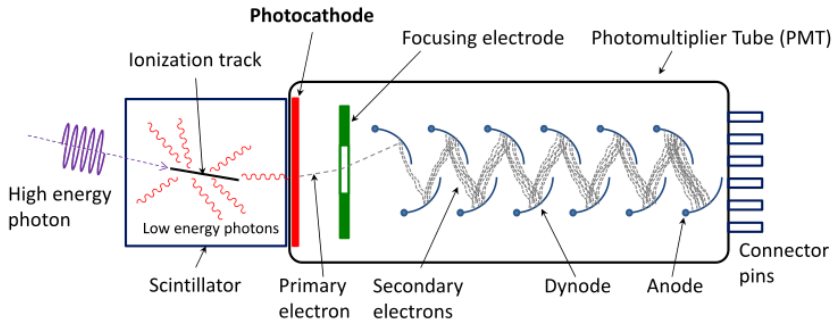

Figure 2.1: Schematic of a photomultiplier tube coupled to a scintillator[14].

A photon usually releases a single photoelectron, which alone is insufficient for detection. Therefore, to amplify the signal, dynodes are used within the PMT to multiply the initial single electron. The photoelectron, drifting towards the anode, encounters a first dynode, where it triggers an avalanche event and releases more electrons, which, again, trigger additional avalanche events at each following dynode with successively higher potential.

The resulting amount of electrons will now have a sufficient impact to be measured as a voltage pulse[14].

2.1.1 Hamamatsu R9420 SEL

The Hamamatsu R9420 is a series of PMTs with high standards in point of linearity, quantum efficiency, a good time resolution and fast response times. The high linearity is necessary for the PMT to handle signals as close as 300 m to the shower core as well as the faint signal of single particles kilometers away[4]. The SEL Series is basically still a R9420, but due to an agreement between Pierre Auger Observatory and Hamamatsu they have a guaranteed lineary specification because of their critical usage. The specifications in detail are shown in the appendix.

Figure 2.2: Hamamatsu R9420.

The circuit diagram of the PMT Hamamatsu R9420 SEL seen in Fig. 2.3 shows the exact amount of eight dynodes. The specified voltage divider ratio demonstrates a progressive change in voltage, ensuring consistent electron acceleration through each dynode stage.

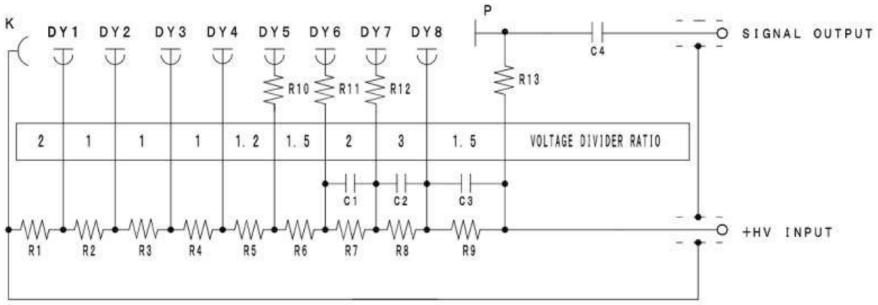

Figure 2.3: Schematics of the Hamamatsu R9420.

This ensures that the electrons drift through the electric field and interact with each dynode. Each resistor and capacitor in the diagram is employed to reduce noise and voltage fluctuation. The last capacitor decouples the positive high voltage for the operation of the PMT from the sensible equipment and reduces the risk of damage or erroneous measurements. In some cases, after high impacts of electrons, it may overcompensate and will end up with a higher offset than the measurement initially starts with. In this, these capacitors are discussed as a possible reason for this phenomenon.

As seen in Fig. 4 the PMT is to be set in two voltages. there is one value for high gain and on for low gain. The high gain delivering an amplification of $7 * 10^5$ is reached on an exact voltage of 1250V. The low gain amplification is $5 * 10^4$ if the voltage is set between 750 V and 950 V . In our test bench the low gain amplification is set with a voltage of $\approx$ 850 V [4].

2.2 Afterpulses

Afterpulses are a well-known type of phenomenon in PMTs. They generate signals not directly related to actual photon interactions at the cathode of the PMT. There are two distinct timeframes for two types of afterpulses. The first type of afterpulses, referred to as latepulses for clarity, is not the subject of this investigation and will hardly be noticed here. These very short delayed "latepulses", as refered to from Photonis, although irritating, may originate from luminous reactions, where light is emitted due to the mass of electrons interacting with dynodes, as shown in Fig. 2.4, and is relatively rather short-term and closer to the actual pulse. Those photons may hit the photocathode and release photoelectrons again[3] [7].

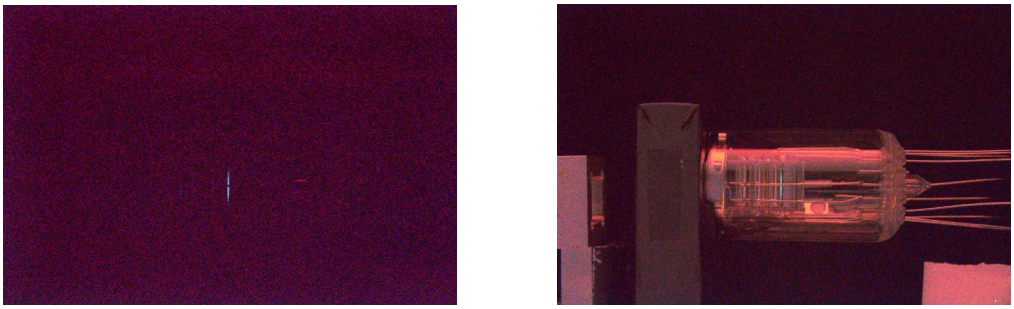

Figure 2.4: Luminous afterpulses of a R9420-100 PMT: The left image shows the PMT's dynodes glowing blue. The right image is a montage highlighting the glow as an overlay[3].

There is also another known explanation for short delayed afterpulses, where electrons hit the dynode and fulfill the circumstances for an elastic impulse. [14][11]

The second type, which this study focuses on, originates from the ionization of the few remaining gas atoms inside the tube within the vacuumed PMT, and will simply be referred to as afterpulses. These afterpulses occur when electrons, moving through the PMT's electric field, collide with residual gas atoms, ionizing them. Resulting in positive charge these ions are forced to drift in the electric field. The force causing the drift of electrons and ions depends only on the charge[5]. However, due to their significantly greater mass, the ions are accelerated more slowly. For example the lightest residual gas molecule is hydrogen with $m_{H_2^+} \approx 3.3 * 10^{-27}$ kg (2u)[8]. The mass of an electron is known to be $m_{e^-} \approx 9.1 * 10^{-31} kg$[6]. With the Coulomb force being the same for an electron and a once-ionized hydrogen ion, the ions are slowed in their drift by a factor of ≈ 4000 relative to the electrons. These drifting ions may now interact with the cathode and potentially release additional electrons, depending on the energy the ion transfers to the cathodes electrons. If the transferred energy at impact is higher than the binding energy of an electron, the electron will behave similar to the photoelectrons, drifting through the field into the dynodes, releasing another secondary emission avalanche of electrons. Interaction with the anode at the end of the PMT will send a signal to the connected measurement system, that will subsequently detect those signals as a distinct pulse. The number of electrons, the form, the delay and the magnitude of the afterpulse are heavily influenced by the type of gas being ionized in the first place[11].

Photonis, also a manufacturer of PMTs and only mentioned here for comparison, provides a useful table outlining the general range of delays for latepulses and afterpulses, as displayed in Fig. 2.5. It shows that residual gases in the electron-optical input system — the part between the cathode and the dynode — have an earlier impact and can be distinguished by their origins, hence the type of ion. H_2^+ (0.3 s), He^+ (0.4 μs) and CH_4^+ (1 μs) result in differently delayed afterpulses. The later impacts of afterpulses might come from ionization that occurred in the dynodes. Afterpulses are specific to the type of PMT due to its physical characteristics and the rest-gas resulting from the production-process. Photonis

afterpulse source	duration (typ.)
luminous reactions	20 to 100 ns
ionization of residual gases:	
- in the electron-optical input system	H_2^+: 0.3 µs
	He^+: 0.4 µs
	CH_4^+: 1 µs
- in the electron multiplier	1 to several µs, e.g. 3 µs for Cs^+

Figure 2.5: Afterpulse Sources [7]

To illustrate some variations, we will be examining information provided by Hamamatsu, the manufacturer of all the PMTs tested in our experimental setup. In the case of Hamamatsus experience the latepulses are observed with a delay in range of several nanoseconds to several tens of nanoseconds, a difference with a factor of roundabout 10 in comparison to the Photonis data, and the afterpulses are delayed with a range of several hundreds of nanoseconds to several microseconds, which is pretty similar to the Photonis data[11].

Therefore, studying these afterpulses in an isolated experimental setup should help determine the timings of these afterpulses. This is crucial for filtering out those afterpulses in actual field measurements and avoiding the processing of false information. Additionally, if we also consider latepulses in this context, they indeed reduce the measurement accuracy. In some cases, blanking or leaving the PMTs inactive for a period long enough to exclude possible secondary afterpulses is necessary[7]. For completeness, it is worth mentioning the phenomenon of prepulses, which can occur when photons miss the cathode and strike the dynode directly, resulting in a relatively weak signal."[10].

2.3 Experimental Setup

The experimental setup, that was developed as part of a master-thesis for the test of the AugerPrime SSD-PMTs [4], is located in the basement of the institute, consisting of a VME-crate, a modular data acquisition system, equipped with transient waveform recorders connected to Photomultiplier Tubes. The system is controlled by a PC connected to a VME-crate that triggers LED pulses to simulate event detections. The NIM module primarily serves as a fan-out to distribute signals to the FADC boards. This setup is designed to capture high-resolution test data from the PMTs which would detect scintillation events caused by particle interactions in the field as intended for the AugerPrime upgrade. More than 1000 PMTs have been tested for the Pierre Auger Observatory in this setup in various settings.

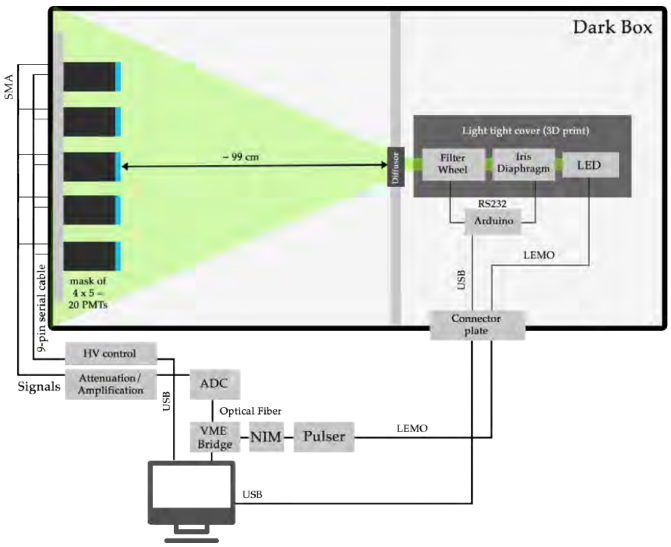

Figure 2.6: Schematic Representation of the PMT Test Setup[4].

The PMTs are mounted in a mask of 4x5 slots, connected to HV control for setting the PMTs up. The signals are splitted and either amplified or attenuated before fed into the analog-to-digital converter to allow a large dynamic range. To prevent the PMTs from damage they are employed and engaged inside the dark box which has to be closed during measuring.

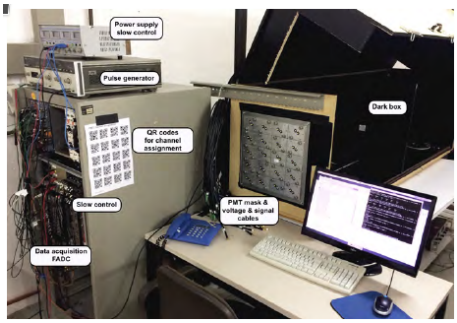

Figure 2.7: Enter Caption

Figure 2.8: Experimental setup overview

2.3.1 Data Acquisition

Data acquisition is performed at a sampling frequency of 100 MHz, ensuring detailed waveform capture. Each measurement session records 5000 pulses per PMT slot, with each file corresponding to a single PMT slot's data collection session. This high rate of sampling allows for precise reconstruction of the timing and magnitude of scintillation events, facilitating detailed analysis of particle interactions within the detectors. Data integrity and synchronization are maintained by a dedicated timing system integrated within the VME crate. The ROOT files follow a cyclical naming pattern:

BatchNN_MM_XX_YY_Pulses.ROOT

- NN $\in [01 : 80]$ represents the batch number.
- MM indicates the voltage used to setup the PMT, either LG (Low Gain) or HG (High Gain). (see Sec. 2.1.1)
- XX shows the iris diaphragm setting, which in the test data had been adjusted from opened up at 100 down to 20 and has particular settings either for LG or HG.
  - For LG, the settings include 89, 92, 95, and 100.
  - For HG, the settings are 20, 25, and 30.

  The reason for this is that at lower gain settings, the PMT also lowers the amplification, hence the pulse would be too insignificant. For the higher voltage setting, and due to the higher amplification, we need to close the iris diaphragm to protect the PMT from possible damage.
- YY refers to the filter wheel, having 10 Options. Beginning from 10 the strongest filter, lowering down to 1 the weakest one.

An example for a typical file name would be Batch80_HG_20_10_Pulses.ROOT. It contains data of the pulse measurement of the 80th batch of 20 PMTs on high gain voltage setup, and the LED light pulse filtered by an iris diaphragm set at 20, and the filter wheel set to option 10.

2.3.2 Filter Wheel and Iris Diaphragm

As already seen in the build of the darkbox the LED exposing the PMTs to light undergoes attenuation by two components. Initially the light through a motorized filter wheel with ten positions used in our test.

Figure 2.9: Filter wheel FW212 CW in its housing (left) and removed from housing (right)[4].

Figure 2.10: Iris diaphragm in its device (left) and isolated (right) [4]

Both can be controlled from the PC. While the filter wheel is used to switch between filters, the diaphragm can be varied in small steps individually by an electronic motor. It cannot be overlooked that, following attenuation, the LED beam is further refined through a "Butterbrotpapier"-diffusor[13], ensuring a more uniform light distribution before it interacts with the PMTs.

Chapter 3

Methods

3.1 Phase I: Initial Data Preparation and Visualization

The initial phase of this study focuses on the enumeration and extraction of data from ROOT files associated with the pulse testing of PMTs.

3.1.1 PMT Data File Integrity

Each ROOT file is verified to contain the same amount of measurements and maintain a consistent sampling rate, which will be crucial for ongoing analysis. Therefore a python script has been developed.

Checking each of these files with as well developed python scripts showed that there is indeed consistency in all the measurements. The measurements are recorded in nanoseconds (ns) and start at $t = 5$ ns and end at $t = 10235$ ns, having a a continuous sampling rate of 10 ns. Therefore the 10 MHz sampling rate is confirmed.

3.1.2 Data Smoothing and Frequency Analysis Techniques

After initial visualizations, it was decided to apply a running average to the data beforehand starting from Chapter 3.2, if not indicated otherwise. A frame of values next to the initial value will be defined. The mean value of those reverts to the starting y-value, resulting in much smoother data and an initial reduction of noise[12].

$$\mathrm{SMA}_k = \frac{p_{n-k+1} + p_{n-k+2} + \cdots + p_n}{k} = \frac{1}{k} \sum_{i=n-k+1}^{n} p_i \tag{3.1}$$

As part of data preparation FFT scripts have been developed to filter out frequencies, after preparing the data with running average at a window size of n = 5. These scripts aim to remove frequencies originating from external sources or even the equipment used in the testing bench that may corrupt the data. In this study, the numpy FFT function was used for one-dimensional data along a time axis, based on:

$$A_k = \sum_{m=0}^{n-1} a_m \exp\left(-2\pi i \frac{mk}{n}\right), \quad k = 0, \ldots, n-1. \tag{3.2}$$
$$with : a_m = \exp\left(2\pi i f_m \Delta t\right)$$

The Discrete Fourier Transform (DFT) is the summation of complex exponentials, showing the discrete frequency components of the signals. Initially the analysis was focusing on the latest row of measurements labeled "Batch 80", therefore, and due to the high amount of workload, the FFT scripts had been applied on this batch of PMTs exclusively. The frequency indices had been transferred into real frequencies for easier analysis. The plots showed no frequencies disturbing the data. Exemplary two different PMTs in different settings will be displayed in Fig. 3.1 and Fig. 3.2. The first of those two PMTs, ons mounted at slot T08, operated in a High Gain setting with the Iris at 20, while the other, mounted at slot T20, ran in Low Gain with the Iris set to 100. Both PMTs were positioned behind the filter wheel set to position 1.

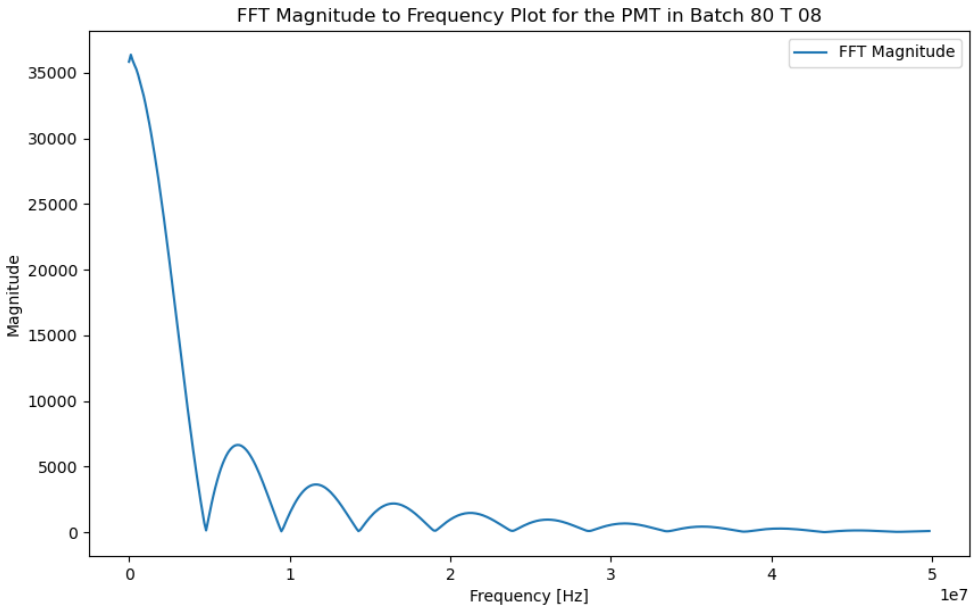

Figure 3.1: High gain channel of PMT position T08 with settings: Iris 20, Filter 1

After revising all of the pulses in FFT mode it can be confidently stated that under normal operating conditions the equipment does not produce frequencies that require filtering. Noteable, there are, indeed, variations in the magnitudes. These correlate heavily with the settings, gain, iris configuration and the filter wheel position.

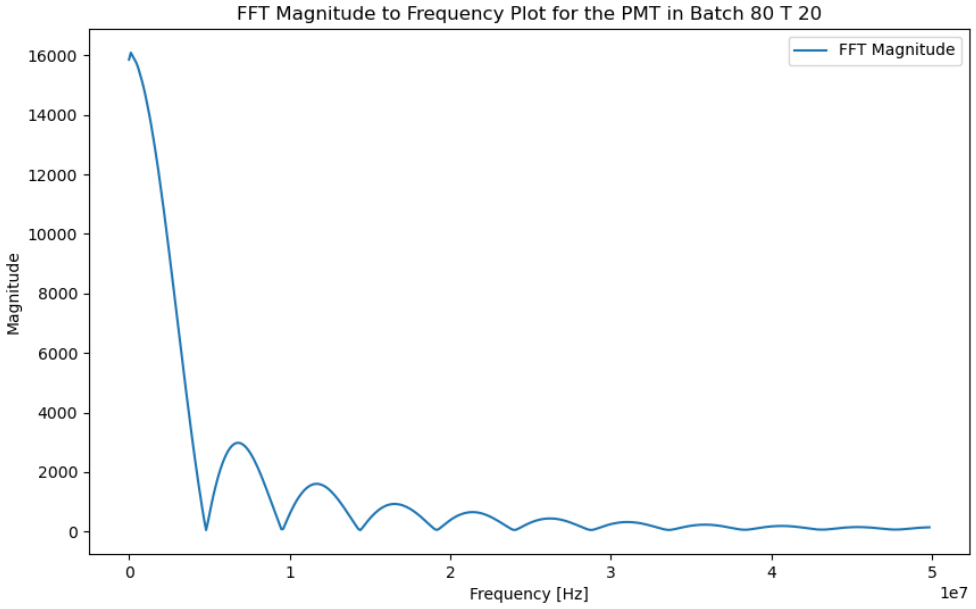

Figure 3.2: FFT Plot of the PMT20 in Low Gain setting. *iris setting: 100, filter wheel: 1*

3.2 Phase II: Strategic Exclusion of Anomaly-Affected Slots

3.2.1 Analysis of Empty Trace Occurrences in PMT Data

To exclude the light pulse or its generating as an isolated error for future trouble shooting of the testing bench and to get more information about the behaviour of the PMTs the traces without any main pulse, as seen in Fig. 3.2.1, have been identified with precision from all of the PMTs. An example, same setting, of a successful measurement can be seen in Fig. 3.2.1. The data of failed pulses were excluded from all further observations, unless otherwise indicated.

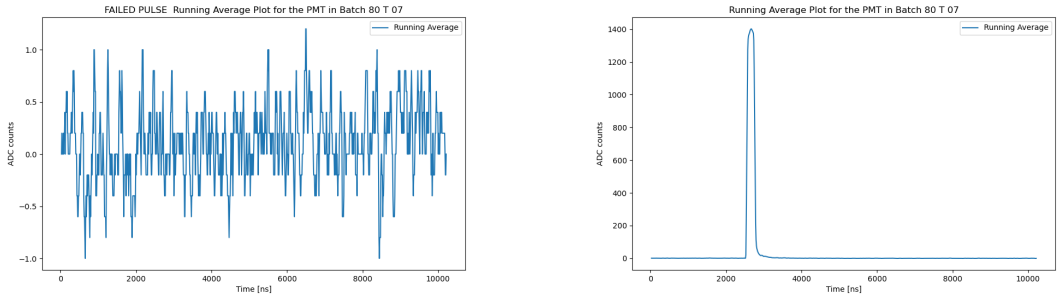

Figure 3.3: Comparison of ths single traces of measurement 302 (left) and measurement 303 on high gain, iris 20, filter 1 settings.

PMT	Count	PMT	Count	PMT	Count	PMT	Count	PMT	Count
PMT 01	292	PMT 05	180	PMT 09	224	PMT 13	437	PMT 17	355
PMT 02	313	PMT 06	176	PMT 10	255	PMT 14	380	PMT 18	362
PMT 03	305	PMT 07	247	PMT 11	372	PMT 15	366	PMT 19	304
PMT 04	328	PMT 08	318	PMT 12	417	PMT 16	298	PMT 20	228

Table 3.1: Empty Traces per PMT Slot

The empty traces, as listed in Tab. 3.1, were explicitly identified and could be excluded.

On a little side note, slot T04 seemed to be off for batch 80, 79 and 78. with other settings than used in this subsction.

3.2.2 Investigation of Displaced Main Pulses

Investigating the batch 80 measurements with the iris set to 20 and 30, other irregularities were identified. The presence of flat lines at certain points where the main pulse should occur, in every slot of each batch of course lead back to empty traces in Sec. 3.2.1. The interpretation of these visuals is that some of those 5000 measurements would not contain any pulse. As seen in the the example Fig. 3.2.2 there is a thin line beneath the actual main pulse around 2550 ns – 2750 ns. In this plot of 5000 overlayed traces, all representing their own measurement, it is evident that there is a possibility of no pulse for some measurements.

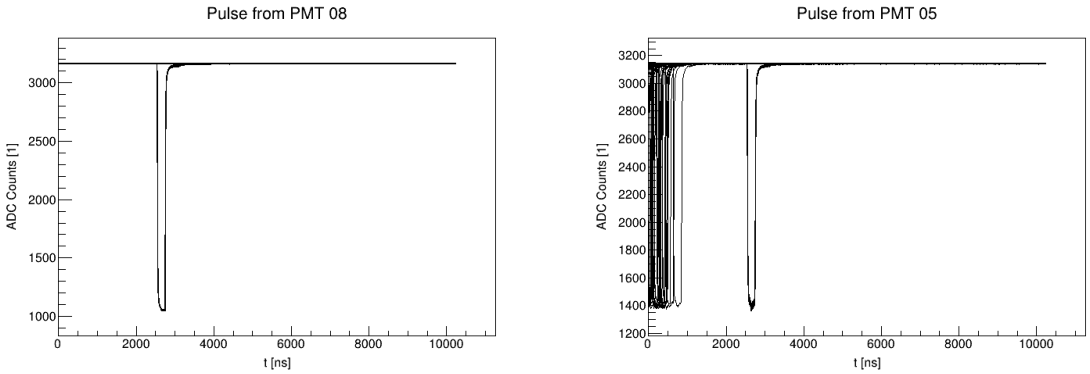

Figure 3.4: An overlay for all measurements of the PMT in slot T08 (left) and in T05 (right) of the 80th batch. *Settings: High Gain, Iris 30, Filter 1* note: The thin lower line beneath the pulse, in addition to representing displaced main pulses, also indicates the possibility of missing pulses as discussed in Sec. 3.2.1

Looking at other slots, like at the PMT at slot T05 in the same batch Fig. 3.2.2 we can even see singular pulses being irregularly advanced on the time axis. Further investigations of all the batches showed that we see this behaviour on exclusive slots only, independent of the mounted PMT. The first six slots are inflicted by this type of late measurements in almost every batch. An estimation have been made by looking over all the 62 batches for the HG channel and the iris configuration 20 and the filter wheel on position 10, where 95% of the first six slots do show various early pulses due to a measurement shift. Therefore it is evident that we are not seeing early laser pulses or PMT relevant effects, since the other parallel installed PMTs do not show any kind of similar behaviour. These slots will be permanently excluded from investigating for afterpulses on different PMTs.

The light pulse itself is not the reason for the the missing signals, at least not alone. Ignoring the PMTs from slot T01 to T06, where the early pulses occur: The counted appearances of empty traces in a cycle of 5000 light pulses vary from at least 224 to 362 across the different slots in one batch. For those six ignored slots the range is even wider. The PMT in slot 6 for example has only 176 empty traces. In this quick analysis the early pulses are not classified as an empty trace, although missing the correct timing for the main pulse. The fact that the PMT in slot T06 records the fewest empty traces despite its late measurements suggests that similar reasons may underlie the empty traces in other slots, possibly indicating generally delayed measurements.

3.2.3 Analysis of Unusual Signal Behavior at 9000 ns

Another irregularity occurs, when looking at the measurements for each slot of batch 80 at the high gain setting with the iris set to 20 and 30 for the highest filter wheel setting 10. The summed up traces for each PMT Slot will be investigated. At approximately 9000 ns after the start of the measurement there are odd phenomena. The phenomena varied across the different slots of the batch. In some cases the summed up pulse traces were unremarkable at this timestamp and showed expected noise and offset. However there are remarkable small pulses at other slots potentially worth investigating. Other PMTs in this measurement showed the exact opposite

behaviour: negative pulses. There may be an option of overshooting right after big impacts or different features of the hard- or software, but a classical photon-indicated pulse in the PMT should not make a measurable distinct singular reversed pulse.

This lead to further investigation. If these pulses depend on specific PMTs, it would be crucial for the Pierre Auger experiment to be informed.

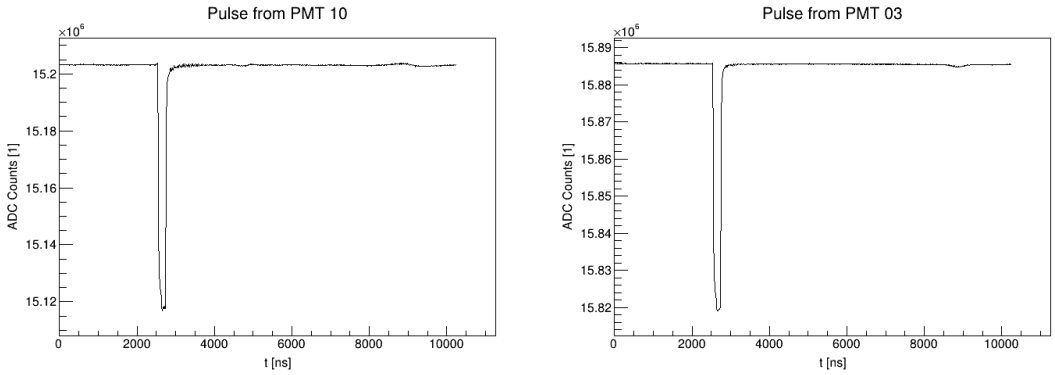

Figure 3.5: The assumingly slot related signal phenomena. Looking at batch 70, gigh gain, isis 20 and filter 10. Slot T10 the left and slot T03 on the right.

To clarify if this is setting-related, if it is a PMT-correlated observation, or a slot related one. Eighteen slots have been observed, since two had to be ignored due to . There is a very high correlation between these pulses around 9000 ns and the slots used. Across varying settings and batches, six slots always showed unanticipated pulses with the same polarity. If there was, for example, a positive pulse at slot T10 , as showed in Fig. 3.2.3, it has been a positive pulse for this slot at all other batches and settings investigated. If there was a negative pulse, like for slot 3 in Fig. 3.2.3, in the same direction as the actual pulse, it stayed negative at 9000 ns for the other settings. This suggests a potential linkage between the slots. Due to the small scale of the analysis, this pattern of irregularities is not yet substantiated. The validity of this potential linkage is already challenged by exceptions in two slots that vary their behaviour depending on the setting. A more systematic investigation would be needed.

It also turns out that these phenomena are only to be seen with the high filter set up. Either it does not occur on lower filter settings, or the signal and noise where higher on lower filter wheel settings.

A slightly more detailed investigation of this 9000 ns phenomena lead to the observation that the phenomena can have different effects. In this analysis we zoomed in at the not yet explainable pulses at 9000 ns and checked the variances of it using the numpy function VAR() without the "Bessel's correction"[16], as in:

$$\frac{1}{N}\sum_i |a_i - \bar{a}|^2 \tag{3.3}$$

While some slots show a peak in the mean value around 9000 but a stable spread, as seen in Fig. 3.7, others show no effect in the mean value but in increase in the spread at 9000ns, as seen in Fig. 3.6.

Exemplary plots of the subtle and conspicuous phenomena around 9000 *ns and their variances (Setting: High gain, iris 30, filter 10,* $t = [8500\ ns : 9500\ ns]$*, running average window = 5):*

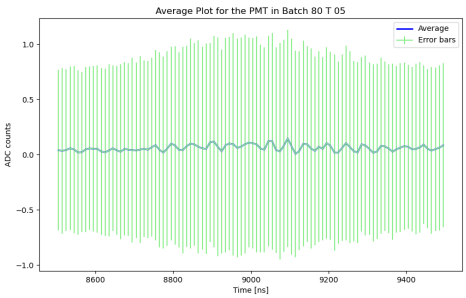

Figure 3.6: An example of a hidden unclear 9k-phenomena, slot T05

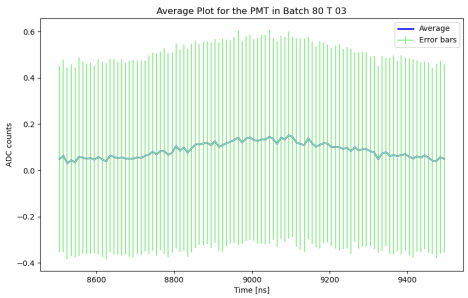

Figure 3.7: An example of a visible 9k phenomena, slot T03

Although further investigation into this phenomenon is not pursued, no evidence of it being related to PMTs could be found. Due to the prominent appearance of these pulses, suggesting a connection to the slot rather than the PMTs themselves, these slots will be excluded from further analysis. These peaks will not be addressed in this study furthermore.

3.2.4 Examination of Unconfirmed Afterpulses with Increased Light Filtering

Using the same script to overlay all traces from a single PMT slot in another setting shows potential afterpulses. This study instead indicates that we are observing other anomaly effects than the afterpulses anticipated. The setting, in comparsion to the setting in subsection 3.2.2, is mostly remaining unchanged across all 20 PMTs of this batch, only the filter wheel position is changed from position 1 to position 10 for reduced light exposure. The plots indicate afterpulses in a plausible time region.

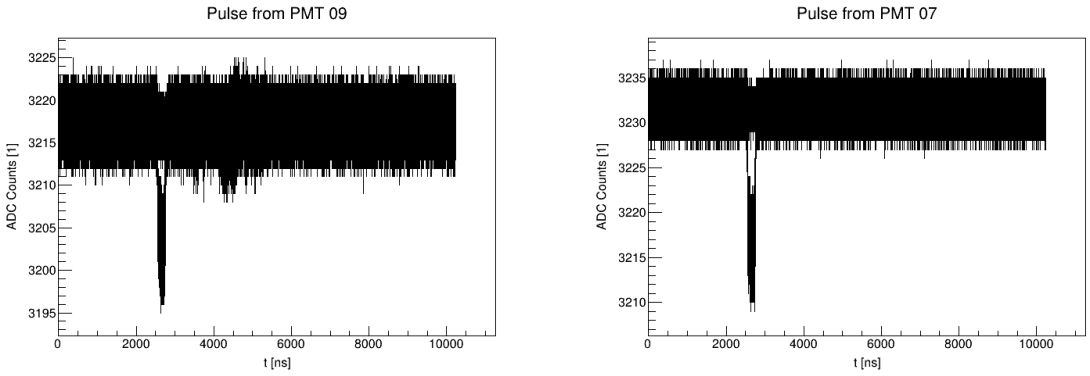

Figure 3.8: Overlayed plots: Exemplary irregularities and potential afterpulses at circa 5000 ns (left: PMT in T09), no anomalies (right: PMT in T07)for the High Gain channel, the iris set up to 20 and the filter wheel to 10

It stood out that those potential afterpulses could not be detected for all of the PMTs in this batch. The exemplary plots in Fig. 3.8 illustrate some bulkiness over the rather noisy signal in the higher filtered signals with smaller peaks. To ensure this slots exclusive behaviour is not a systematic pattern, but actual afterpulses happening, further investigation had to be made.

The focus remains on measurements with the filter wheel set to 10, since the signals of the singular traces seem to be easier to distinguish from potential afterpulses. Although more noisy, the curve flattens out quicker. A script was developed to analyze all High Gain measurements across all batches, even though this setting is not useful for the detection of afterpulses, it still provided valuable insights. Filtering the data from 3850 ns to 8500 ns was decided to avoid unresolved discrepancies at circa 9000 ns Fig. 3.5 and the flattening curve of the main pulse signal, this script was set to find furthermore outliers of the average value of its time position.

It is important to note that, the focus of this analysis is not on ADC counts or signal intensities themselves. The purpose of this analysis is to determine where on the x-axis (time [ns]) the y-values (signal [ADC-Counts]) exceeded the trace's isolated average between 3250 ns and 8500 ns as seen in Fig. 3.2.4. This script includes empty traces, that could maybe as well lead to those peaks, since the origin is not well understood and would need further investigations. Especially checking upon those pulses in even empty traces, which would most likely exclude all possible PMT related options, would be interesting.

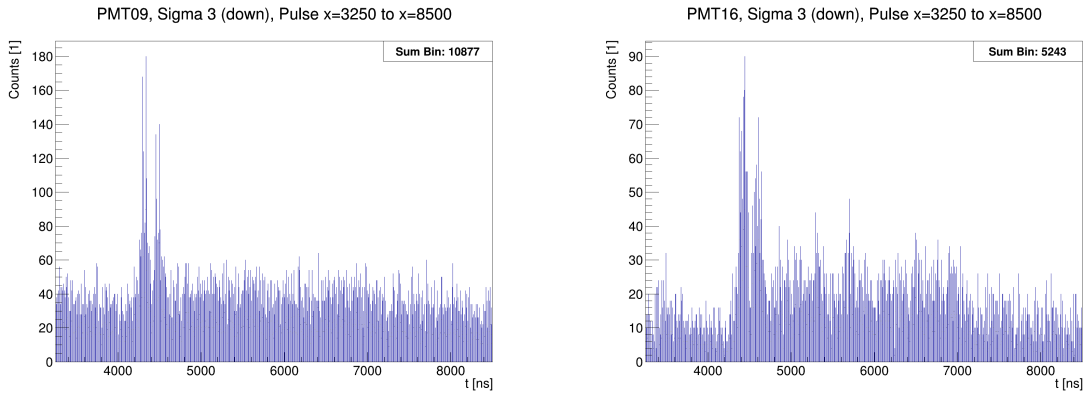

Figure 3.9: Histograms: Counts of measurements exceeding 3σ from each trace's average per time interval. Settings: High Gain, Iris 20, Filter 10; Batch 80 (left) and batch 28 (right)

This script was used on all batches and for all settings. The summary of this analysis, as seen in the table Tab. 3.2, clearly demonstrates a strong correlation throughout the slots, indicating that these additionally measured pulses are not related to the PMTs directly.

These peaks could either be slot-related, due to electrical interactions between the devices or similar, or dependent on the intensity of light reaching the PMT cathode, which varies significantly based on the PMT's position in the grid. As seen in Fig. 3.11

PMT	Count	PMT	Count	PMT	Count	PMT	Count	PMT	Count
PMT 01	0	PMT 05	0	PMT 09	184	PMT 13	19	PMT 17	3
PMT 02	0	PMT 06	0	PMT 10	185	PMT 14	179	PMT 18	0
PMT 03	0	PMT 07	0	PMT 11	170	PMT 15	109	PMT 19	0
PMT 04	0	PMT 08	0	PMT 12	177	PMT 16	172	PMT 20	0

Table 3.2: Counts of events exceeding 3σ from the mean for each PMT between 3250 ns and 8500 ns.

Referring to already made tests[4] regarding the inhomogeneity of the light distribution to the PMTs, as seen in Fig. 3.10, the PMT slots in the middle in fact could have a higher potential for creating afterpulses. However, upon examining the PMT slotss that exhibited these yet-to-be-understood pulses, it was noted that they range from 9 to 16, corresponding to two parallel rows. The slot with the weakest light exposure from those eight slots that lead to those pulses is slot T16. Slot T16 has a light exposure of circa 81,79% of the maximum exposure. Yet, in 186 unique setups with 5000 measurements each, through all 62 batches with available data in the three checked settings, as revealed by scripts and represented by histograms, we have a quota of approximately 92,5% to actually detect those potential afterpulses. There are six other slots with higher potential light exposure than the one for slot T16. Some slots that never showed these phenomena had rates of up to 96.15%.

The peak to peak difference in ADC counts is displayed in Tab. 3.2.4. Exemplary each PMT in batch 80 with the iris set to 20 has been analyzed. A relative overview is displayed in Tab. 3.2.4. The PMT in slot T15, as one of the PMTs between slot T09 to slot T16 with the unusual peaks, only gained 70% of the maximum measured light exposure in this set. This PMT got exposed to less light than 9 other PMTs in this set that did not show the peaks currently under investigation. It can be confidently concluded that there is no evidence found in these pulses to be light exposure-related and it is rather unlikely that these are afterpulses. Therefore, we exclude the slots from T09 – T16 from further afterpulse investigation, as the pulses observed in these could compromise the data relevant to afterpulse detection.

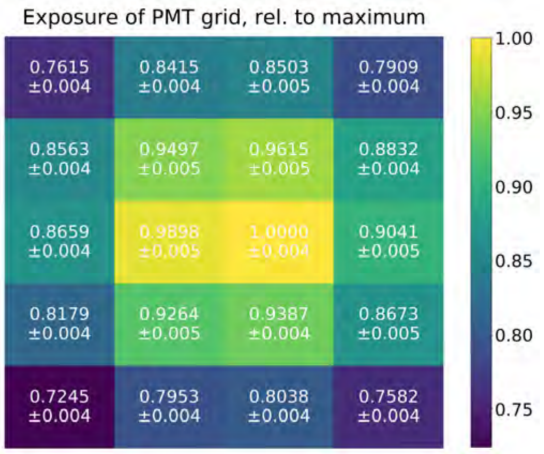

Figure 3.10: Inhomogenity of light exposure [4]

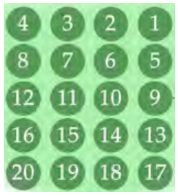

Figure 3.11: Draft of front view of optical path with LED grid and the rest of the build[4]

Peak to peak measurements of ADC counts for each PMT			
T04 = -7.0	T03 = -32.8	T02 = -32.9	T01 = -35.5
T08 = -34.2	T07 = -33.1	T06 = -32.0	T05 = -31.8
T12 = -42.3	T11 = -33.2	T10 = -36.8	T09 = -35.0
T16 = -36.4	T15 = -29.6	T14 = -35.1	T13 = -31.9
T20 = -33.9	T19 = -26.1	T18 = -29.6	T17 = -29.5
$\mu \approx -33.25 \mid \sigma \approx 3.36$ with T4 excluded			

Peak to peak measurements for each PMT related to max peak			
T04 = N/A	T03 = 0.78	T02 = 0.78	T01 = 0.84
T08 = 0.81	T07 = 0.78	T06 = 0.76	T05 = 0.75
T12 = 1.00	T11 = 0.79	T10 = 0.87	T09 = 0.83
T16 = 0.86	T15 = 0.70	T14 = 0.83	T13 = 0.75
T20 = 0.80	T19 = 0.62	T18 = 0.70	T17 = 0.70
with T4 excluded			

Table 3.3: Peak to Peak differences for batch 80 at High Gain with the iris set to 20 and the filter to 10

3.2.5 Closing Analysis: PMT Suitability for Extended Research

Summarizing the data preparation process, this study concludes that, among others, the PMT in slot T07 in batch 80 appears ideal for further investigation of afterpulses.

Additionally at some point of this study attention shifted to measurements with the setting of High Gain with the filter wheel set to 1, from iris to 20 to iris to 30. The phenomena of this unexplainable pulse at 9000 ns Fig. 3.2.3 is not to be seen at this setting in any slot nevertheless. Fig. 3.2.5

Measurement of slot T07 with the following settings: High Gain, iris opened up 30, filter wheel at position 1:

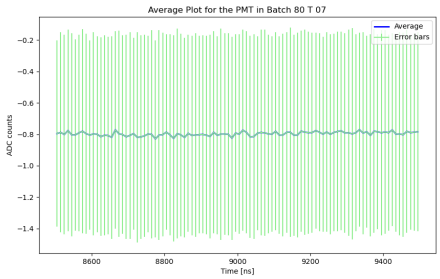

Figure 3.12: Discussed area with a running average of n=5 and error bars representing variances

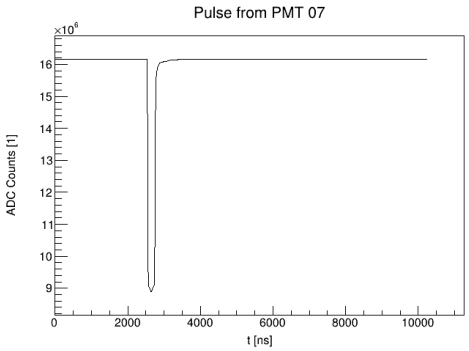

Figure 3.13: Plot of all the measurements summed up, empty traces included

3.3 Phase III: Afterpulse detection

This chapter focuses on examining afterpulses. As demonstrated in other researches, afterpulses are not easily observed without closer inspection. As seen in Fig. 3.14 the first, outer gray plot did not display a lot of details of a potential first afterpulse. The other two potential afterpulses were clearly visible at first sight without further investigation. The inner green plot displays a more zoomed in plot with the peak of the main pulse cut off. The first potential afterpulse can now be identified as anticipated. As well as in the investigation of afterpulses as a part of the PhD thesis of Dr. Sven Querchfeld [3] in the second plot Fig. 3.15 of this chapter it is observed that the pulse is partly masked by the main pulse, potentially complicating the distinction and clear identification of afterpulses.

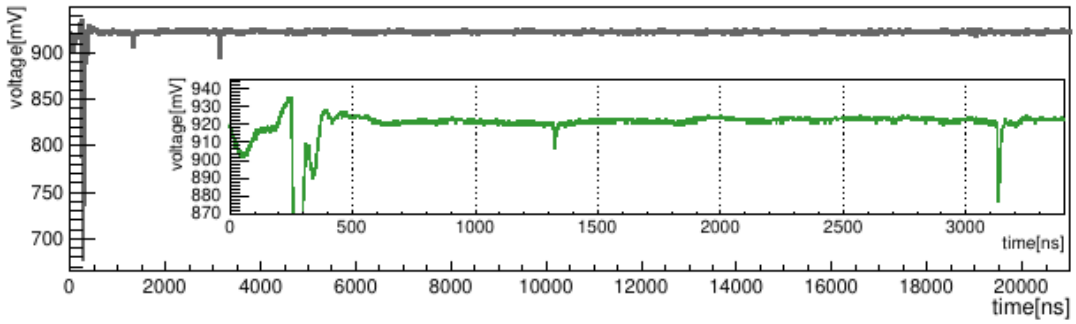

Figure 3.14: A tested waveform with 21μs length [9]

Especially when reminding that those plots are already well worked-out. In case of the red plot seen in Fig.3.15 tha data is taken by measuring a PMT from almost the same as the series this study refers to. The R9420-100 is just a PMT with other specifications for the Pierre Auger Observatory, focusing on the fluorescence detection, the elementary schematic remains the the same. Still one has to point out that the afterpulse phenomena in the r9420 is less prominent than in the so called "super-bialkali" version r9420-100, which tends to more amplified photoelectron multiplication [3].

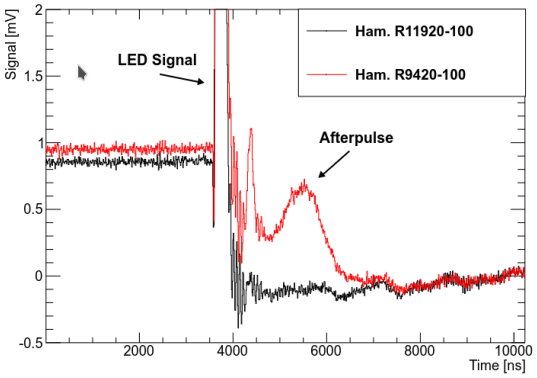

Figure 3.15: Afterpulse comparison of the Hamamatsu R9420-100 (red) and the newer R11920- 100 (black). Shown is the average recorded PMT signal of 1000 LED pulses with a width of 100 n [3]

After focusing on the data of slot T07 PMTs for plots with a lower filter wheel setting and zooming in on the right side at the back of the main pulse, a potential afterpulse could be found. This recalibrating is now applicable at any setting with the filter wheel positioned at 1, in any slot. The following plots display potential afterpulses that are not exclusively slot-related and remind of the afterpulses in other researches by delay and form. As intended before the focus still stays on batch 80, slot T07. For this first measurement no running averages have been applied for further variance investigation.

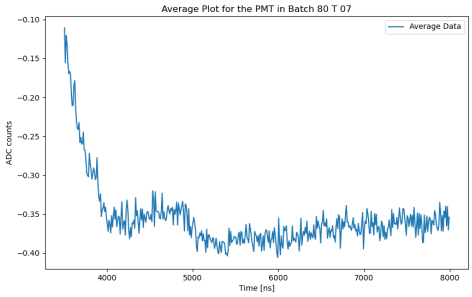

Figure 3.16: Plot for the Low Gain setting with the iris at 89

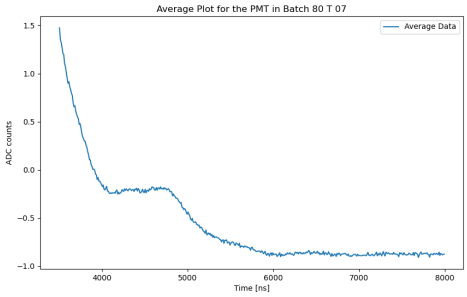

Figure 3.17: Plot for the High Gain setting with the iris at 30

As expected, the plot of the Low Gain measurement is more noisy due to the smaller signal input, as seen in Fig. 3.16. The signal-to-noise ratio changes, typically due to the regular background noise remaining rather stable. Noise is usually originating from various sources starting from electric devices, especially from power supplies, used in this test bench and including environmental factors. Such disturbances can include thermal noise, electromagnetic interference, minor vibrations, which will not be amplified like the signals. Therefore a higher gain, a wider opened iris and a lower filter wheel setting, as seen in Fig. 3.17, is resulting in a higher signal to noise ratio.

A stronger light exposure indicates a relatively higher pulse and a stronger afterpulse as well, as various researches show, and as seen in this study [17] for example. In all cases of the batch 80 an afterpulse indication is visible when the filter wheel set to 1, although those low gain measurements are not ideal due to their insufficient data quality, for example for fitting. The main pulse would be sufficient, but for collecting data about afterpulses we have to look at smaller scales. However, afterpulses are visually detectable even at the lowest setting with Low Gain and the iris set for the highest Low Gain-related light reduction to 89, and, of course, as well with the highest potential signal at the setting on High Gain and the iris opened up to the High Gain-related maximum of 30.

The error bars associated with the aggregated data over 5000 light pulse cycles are considered to be within acceptable limits. Error bars have been set for the average plots including all of the - not empty - 5000 traces. On the big scale the error bars can hardly be seen, due to their small range and that there are 1024 error bars on the graph in Fig. 3.18. As soon as we are looking for smaller scales the error bars seem become prominently large. (See Fig. 3.19 and Fig. 3.20. But further calculations show that the peak to peak value for the complete plot is ≈ 1609 ADC counts. n comparison, the error margins in the three subsequent plots appear more reliable.

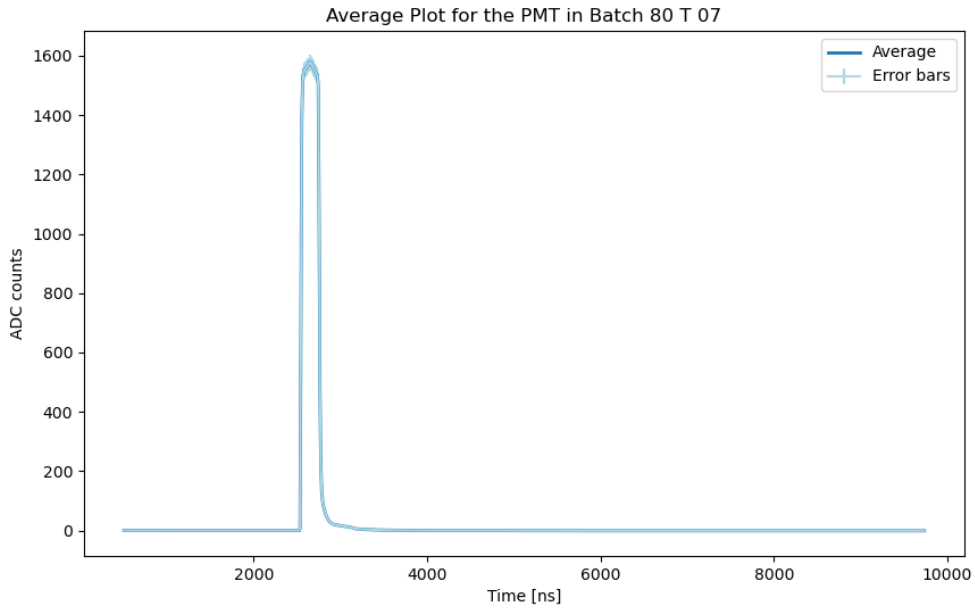

Figure 3.18: standard deviation, High Gain, Iris: 30, Filter Wheel: 1, t=[0ns:10500ns]

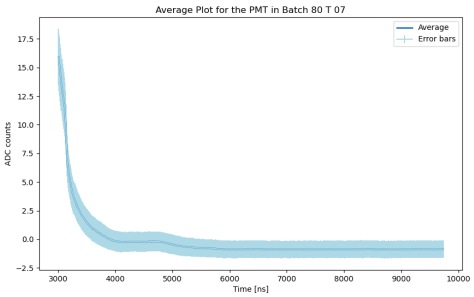

Figure 3.19: Standard deviation, High Gain, Iris: 30, Filter Wheel: 1

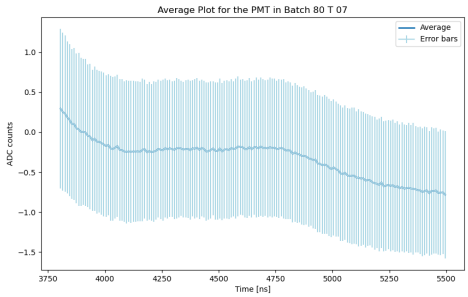

Figure 3.20: Standard deviation, High Gain, Iris: 30, Filter Wheel: 1

The plots displayed are still for the PMT at slot T07. It is the average plot over all visible traces, without moving average and with the setting on High Gain, iris at 30 and the filter wheel set at 1. The maximum height of the error bar in the full scale plot in Fig. 3.18 is ≈ 359 ADC counts. In relation to the peak to peak value of ≈ 1609 ADC counts. The range of almost ≈ 718 ADC counts in relation to ≈ 1609 ADC seem significant. However, this discrepancy primarily arises from a minor timing variation in the main pulse. Without including the plot, another measurement during the main pulse peak, between 2600 ns and 2700 ns, the maximum standard deviation already is at only ≈ 24 ADC counts, sitting on an average ADC count in this time region of ≈ 1567 ADC counts.

The error bars in the other plots are notably smaller if you take the complete scale into relation. Remembering the peak to peak value from 1609 ADC counts we are talking maximum standard deviation of ≈ 2.5 ADC counts for the data in Fig. 3.19 and ≈ 1 ADC count for the data in Fig. 3.20.

This data will now be used for plotting a fit to establish a more defined potential visibility of the afterpulse. An additional pulse would always sit on top of the measured noise, or on top of the measured main pulse. So in this case we see that the afterpulse sits on the back of the slowly flattening main pulse signal. The logical conclusion is, to separate the afterpulse from the decaying main pulse, to substract an approximate fit of the back of the main pulse, extending to the end of the measured data, from the average plot. All ADC count values in the potential afterpulse time frame will be excluded from the fit approximation. Also the moving average is employed again. Through experimentation it was determined that a moving average window of 10 effectively reduced the noisiness observed in small-scale single trace measurements. We are focusing on the data from the PMT in high gain settings and the iris set at 30, with the rest of the settings still unchanged as seen in Fig. 3.22. Still, for exemplaric reasons, the weaker Low Gain plot is delivered in Fig. 3.21

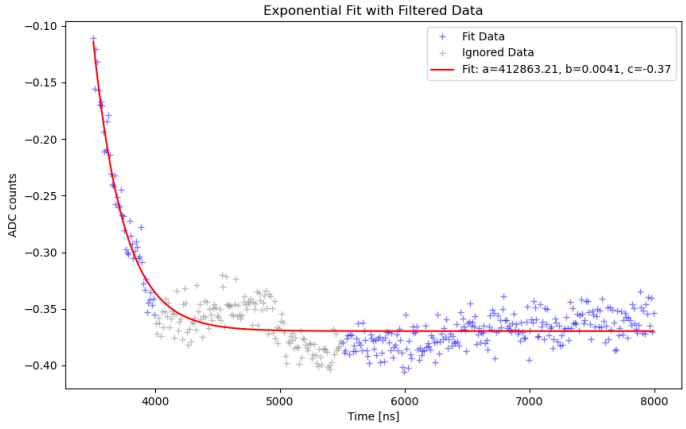

Figure 3.21: Fit for the Low Gain setting with the iris at 89

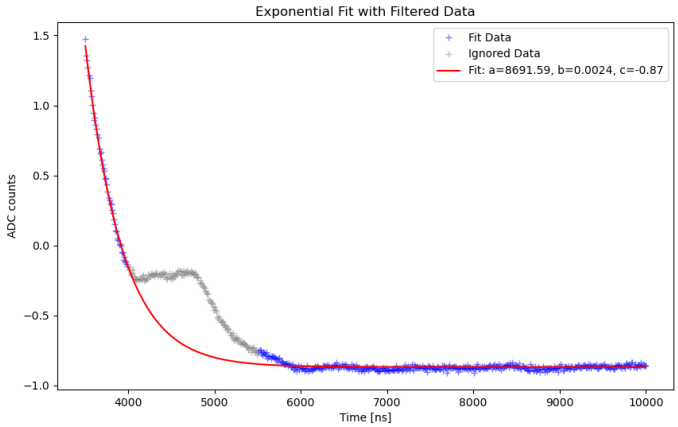

Figure 3.22: Fit for the High Gain setting with the iris at 30

As can be seen the data of the weaker signals have a high degree of variability, making it challenging to fit a reliable model. Even without statistical evidence, a potential afterpulse is already apparent. Therefor the stronger signal, on which will be focused, leads to more stable results. The fit has been chosen to be an approximation of the function:

$$f(x) = a \cdot e^{-bx} + c \tag{3.4}$$

The data has been fitted using the numpy based function `curve_fit` from the `scipy.optimize` package. After fitting the data we will now subtract the fit from Fig. 3.22 from its average plot seen in Fig. 3.17. The result is a clearly visible afterpulse as seen in Fig. 3.23

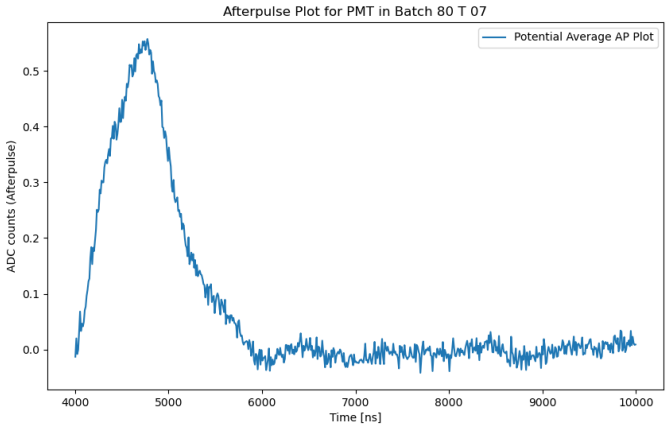

Figure 3.23: Average Afterpulse Visualization for the iris set at 30

A scatter plot, as seen in Fig. 3.3, is displayed for defining and plotting the peak values of each trace minus the fit, in the same setting of Fig. 3.22.

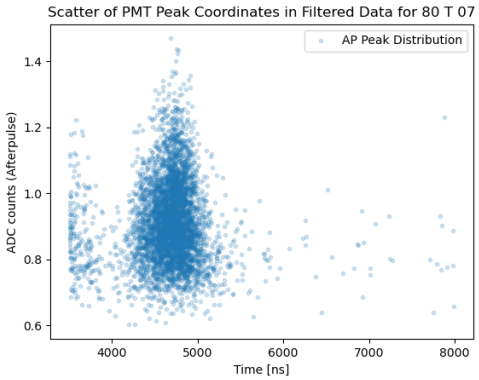

Figure 3.24: Scatterplot of the single traces minus the fit from

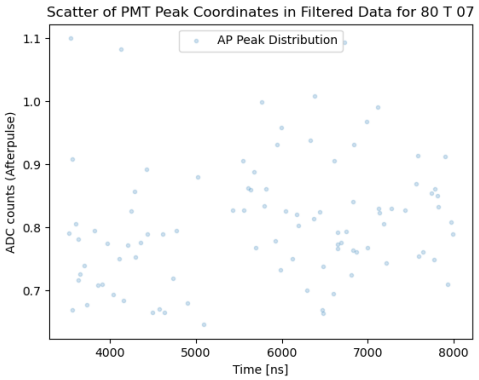

Figure 3.25: Scatterplot, setting on low gain and the iris at 100

As we can now clearly see, again, the analysis of the low gain measurements will still be very complicated. The plot on the right is for comparison only, and did not use all possible measurements, due to computing and workload reasons. It was part of a quick overview and is displayed only for comparison purposes. The same goes out for the other low gain plots. the high gain data was way more interesting and showed clear structures of potential afterpulses.

As a remark, the "AP Peak" dots for timing points before 4000 ns origin from the back of the main pulse and should not be taken as afterpulse information.

Using all of this data, single afterpulses as in Fig.3.26 can be displayed as a result of this study.

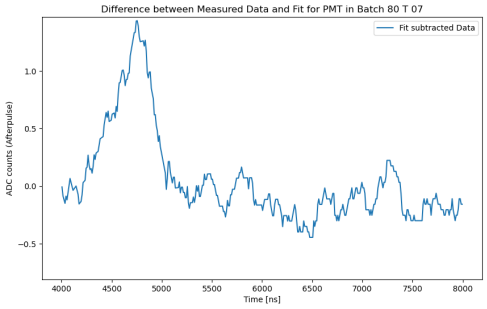

Figure 3.26: Single afterpulse trace in the measurement of batch30

3.4 Phase IV: Characterization of Afterpulses

Having obtained the plots of the afterpulses, this section will now proceed to characterize them.

The scatterplot data can be used for interpretation of distribution and variance of the afterpulse peaks. A script was employed to find the average time point for the peaks between 4000 ns and 5500 ns. The same will be made for the magnitude of the average afterpulse measured in ADC counts as seen in Tab. 3.4 and visualized in Fig. 3.26 .

we continue to focus on the three high gain settings in batch 80, comparing the delay and magnitude of the afterpulse in correlation with the intensity of the main pulse.

The change of the iris setting has impact on the main pulse since the light exposure is varied. Therefore a first hindsight is given that the main pulse has an impact on the amplitude and maybe even delay of the afterpulses. In Tab. 3.4 the data of the average afterpulses of each setting is showed, being displayed in Fig. 3.27 as well.

IRIS Setting	Amplitude (ADC counts)	Time Position (ns)
IRIS 30	0.9077 ± 0.1286	4727.43 ± 326.02
IRIS 25	0.8522 ± 0.1209	4792.64 ± 516.17
IRIS 20	0.8146 ± 0.1181	4835.12 ± 573.94

Table 3.4: Afterpulse Peak Amplitudes and Time Positions for Different Iris Settings

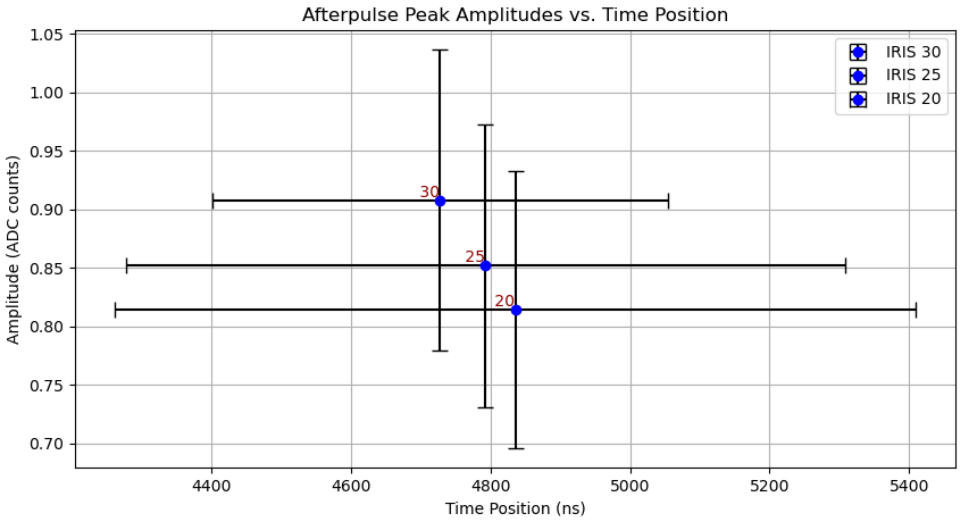

Figure 3.27: Plot of the afterpulse peaks

The afterpulses, as seen in 3.26, are collectively analyzed to determine how the charge of the main pulse affects the appearance of afterpulses. The results can be seen in Tab. 3.5

Table 3.5: Summary of Afterpulses by Iris Setting

Iris Setting	**Total Measurements**
30	107
25	33
20	25

For the peak of the main pulse was determined by taking the average of the offset between 0 ns – 2000 ns and subtracting it from the peak. The ADC counts for the main pulse peak for iris 20 is ≈ -1652, for 25 ≈ -1798 and for 30 ≈ 1832.

Chapter 4

Results

This study successfully prepared the data and identified various false pulses for further investigation and characterization of afterpulses. For further examination, relevant data, with settings or slots excluded from analysis for additional research, has been worked out. Afterpulses have been detected, and their average delay and magnitude were established in relation to the main pulses of the incoming light. Also a link between mainpulse intensity and the amount of afterpulses was analyzed.

Further empirical research can be easily achieved with the developed scripts, so this work lays a solid foundation for future, more advanced empirical and statistical research regarding the analysis of afterpulse behavior of PMTs used at the Pierre Auger Observatory.

Name, Vorname: .....

Erklärung

Pflicht gem. § 13 Abs. 9 PO (Allgemeine Bestimmungen)

Hiermit erkläre ich, dass ich die von mir eingereichte Abschlussarbeit (Bachelor-Thesis) selbständig verfasst und keine anderen als die angegebenen Quellen und Hilfsmittel benutzt sowie Stellen der Abschlussarbeit, die anderen Werken dem Wortlaut oder Sinn nach entnommen wurden, in jedem Fall unter Angabe der Quelle als Entlehnung kenntlich gemacht habe.

....
Datum Unterschrift

Erklärung

Hiermit erkläre ich mich damit einverstanden, dass meine Abschlussarbeit (Bachelor-Thesis) wissenschaftlich interessierten Personen oder Institutionen und im Rahmen von externen Qualitätssicherungsmaßnahmen des Studienganges zur Einsichtnahme zur Verfügung gestellt werden kann.
Korrektur- oder Bewertungshinweise in meiner Arbeit dürfen nicht zitiert werden.

....
Datum Unterschrift

Appendix

SLOT	y_min[ADC]	y_max[ADC]	Delta[ADC]
T1	3059.2	3094.7	-35.5
T2	3163.5	3196.4	-32.9
T3	3150.5	3183.3	-32.8
T4	3173.5	3180.5	-7.0
T5	3117.6	3149.4	-31.8
T6	3074.4	3106.4	-32.0
T7	3206.3	3239.4	-33.1
T8	3138.3	3172.5	-34.2
T9	3192.3	3227.3	-35.0
T10	3015.1	3051.9	-36.8
T11	2999.4	3032.6	-33.2
T12	2980.6	3022.9	-42.3
T13	2632.6	2664.5	-31.9
T14	3014.3	3049.4	-35.1
T15	3017.6	3047.2	-29.6
T16	3094.2	3130.6	-36.4
T17	3206.7	3236.2	-29.5
T18	3211.6	3241.2	-29.6
T19	3157.0	3183.1	-26.1
T20	3180.4	3214.3	-33.9

Table 4.1: Zusammenfassung der Differenzen zwischen y_min und y_max für verschiedene Tests

TECHNICAL INFORMATION

TENTATIVE
Feb. 2018

R9420 SEL

For Pierre Auger Observatory, Fast time response,
38 mm (1.5 inch) Diameter, Bialkali Photocathode, 8-stage, Head-On Type

GENERAL

Parameter		Description / Value	Unit
Spectral Response		300 to 650	nm
Peak Wavelength of Cathode Radiant Sensitivity		420	nm
Window	Material	Borosilicate glass	-
	Shape	Plano concave	-
Photocathode	Material	Bialkali	-
	Minimum Effective Area	ϕ34	mm
Dynode Structure / Number of Stages		Linear Focused / 8	-
Operating Ambient Temperature (with Socket)		-30 to +50	°C
Storage Temperature (w/o Socket)		-80 to +50	°C
Suitable Socket		E678-12A	-
Recommended Supply Voltage between Anode and Cathode		1300	V

MAXIMUM RATINGS (Absolute Maximum Values)

Parameter		Value	Unit
Supply Voltage	Between Anode and Cathode	1500	V
	Between Anode and Last Dynode	350	
Average Anode Current		0.1	mA

CHARACTERISTICS (at 25 °C)

Parameter		Min.	Typ.	Max.	Unit
Cathode Sensitivity	Luminous (2856K)	120	-	-	µA/lm
Cathode Blue Sensitivity Index (Cs 5-58)		9.0	11.0	-	-
Cathode Radiant Sensitivity (at 400 nm)		-	88	-	mA/W
Quantum Efficiency (at 500 nm) (Guaranteed)		18	-	-	%
Anode Sensitivity	Luminous (2856K)	-	50	-	A/lm
Ebbv (Nominal Voltage)	Gain $5x10^4$	750	-	950	V
	Gain $7x10^5$	-	1250	-	V
Ebbi (Dark Current at Ebbv)*	Gain $5x10^4$	-	3.0	10	nA
	Gain $7x10^5$	-	6.0	-	nA
Anode Output Rise Time at Ebbv (for Gain $5x10^4$) (Guaranteed)		-	-	5.0	ns
Pulse Linearity at Ebbv(for Gain $7x10^5$) (± 5% deviation) ** (Guaranteed)		150	-	-	mA
Cathode Uniformity in effective area (at 500 nm) (Guaranteed)		-25	-	25	%

NOTE: Anode characteristics are measured with the special voltage distribution ratio (Tapered ratio) and supply voltage shown next page.
NOTE*: Measured after 30min storage in the darkbox.
NOTE**: Detailed conditions are described on the next page.

HAMAMATSU
PHOTON IS OUR BUSINESS

TECHNICAL INFORMATION

TENTATIVE
Feb. 2018

R9420 SEL

VOLTAGE DIVIDER RATIO AND SUPPLY VOLTAGE

Electrodes	K	Dy1	Dy2	Dy3	Dy4	Dy5	Dy6	Dy7	Dy8	P
Ratio	2	1	1	1	1.2	1.5	2	3	1.5	

Supply Voltage: 1300 V, K: Cathode, Dy: Dynode, P: Anode

CONDITION (for measuring pulse linearity)

1. Pulse linearity is measured with following divider circuit.
2. Pulse width of light source is 50 ns and repetition of light pulse is 100 Hz.
3. Supply nominal voltage for Gain $7x10^5$.

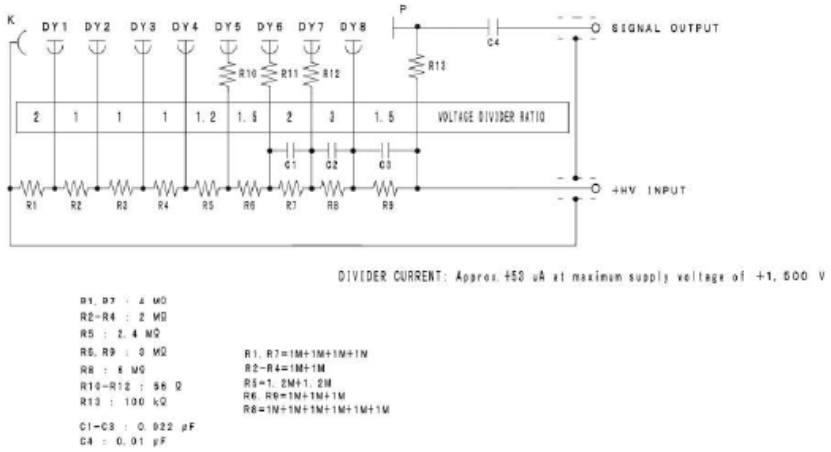

Figure 1: divider circuit

DATA ATTACHED (Following data is attached with a PMT.)

Cathode Sensitivity (Luminous), Cathode Blue Sensitivity Index, Anode Sensitivity (Luminous), Ebbv (Voltage for Gain = $5x10^4$ and $7x10^5$) and Ebbi (Dark Current at Ebbv for Gain = $5x10^4$ and $7x10^5$)

HAMAMATSU
PHOTON IS OUR BUSINESS

TECHNICAL INFORMATION

TENTATIVE
Feb. 2018

R9420 SEL

DIMENSIONAL OUTLINE

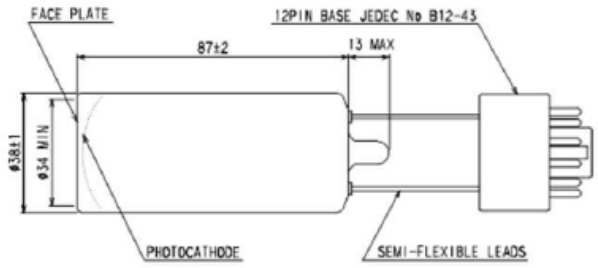

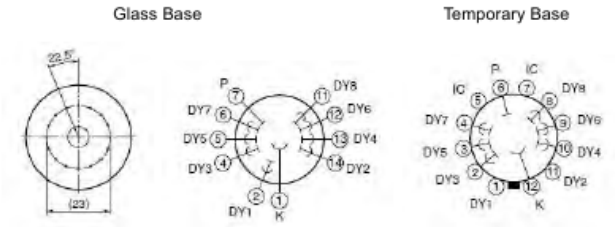

Figure 2: Dimensional Outline and Basing Diagram (Unit: mm)

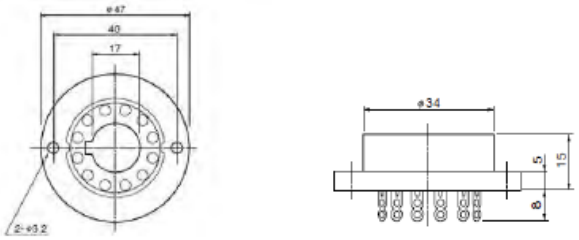

Figure 3: Socket E678-12A (Unit: mm)

NOTES

The material in the R9420 contains Copper-Beryllium (CuBe) Alloy. Please follow the applicable regulations regarding disposal of hazardous materials and industrial wastes in your country, state, region or province.

List of Figures

List of Tables

Bibliography

[1] Antonella Castellina for the Pierre Auger Collaboration *Highlights from the Pierre Auger Observatory* https://doi.org/10.48550/arXiv.1909.10791

[2] Wikipedia *Photoelectric Effect* https://en.wikipedia.org/wiki/Photoelectric_effect

[3] Sven Querchfeld *Detector performance and upgrades of the Pierre Auger Observatory* Afterpulses - Chapter 4.2.4 p.28

[4] Simon Strotmann *Development and First Results of a Test Bench for the Characterization of the AugerPrime PMTs* https://astro.uni-wuppertal.de/fileadmin/physik/astro/mainpage/publications/theses/Master/Strotmann-Master.pdf

[5] Wikipedia *Coulomb's Law* https://en.wikipedia.org/wiki/Coulomb%27s_law

[6] Wikipedia *Electron mass* https://en.wikipedia.org/wiki/Electron_mass

[7] Photonis - *Photomultiplier Tube Basics* Chapter 7, p.17 https://psec.uchicago.edu/library/photomultipliers/Photonis_PMT_basics.pdf

[8] Wikipedia *Atomic mass* https://en.wikipedia.org/wiki/Atomic_mass

[9] Rong Zhao Jr - Afterpulse measurement of JUNO 20-inch PMTs https://arxiv.org/abs/2207.04995

[10] Wikipedia - *"Pulse Behaviour"* https://de.wikipedia.org/wiki/Photomultiplier#Pulsverhalten

[11] Hammamatsu *PHOTOMULTIPLIER TUBES Basics and Applications* Chapter 4.3.8, p.79 https://www.hamamatsu.com/content/dam/hamamatsu-photonics/sites/documents/99_SALES_LIBRARY/etd/PMT_handbook_v4E.pdf

[12] Wikipedia *Moving Average* https://en.wikipedia.org/wiki/Moving_average

[13] K.-H. Becker *Construction and Design*, 2018

[14] Wikipedia *Photomultiplier Tube* https://en.wikipedia.org/wiki/Photomultiplier_tube

[15] Numpy *Routines FFT* https://numpy.org/doc/stable/reference/routines.fft.html

[16] Numpy *Statistics Var()* https://numpy.org/doc/stable/reference/generated/numpy.var.html

[17] Rong Zhao *Afterpulse measurement of JUNO 20-inch PMTs* https://doi.org/10.48550/arXiv.2207.04995